Journal of Materials Chemistry A

Accepted Manuscript

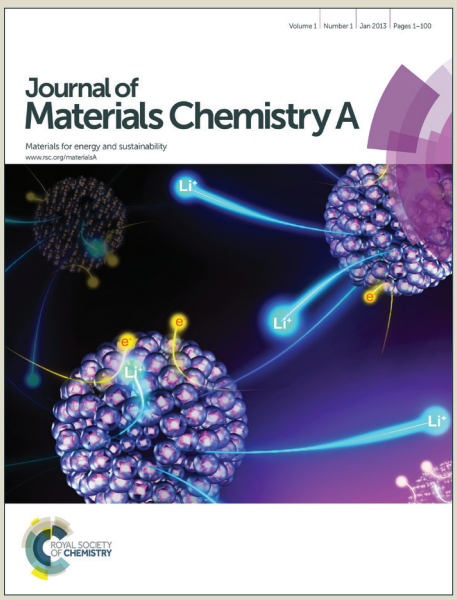

ROYAL SOCIETY OF CHEMISTRY

www.rsc.org/materialsA

Journal of

Materials Chemistry A

RSCPublishing

paper

Surface fluorinated $LiNi_{0.8}Co_{0.15}Al_{0.05}O_2$ as positive electrode material for lithium ion batteries

Cite this: DOI: 10.1039/x0xx00000x

Lei Zhu[a,b], Yang Liu [b], Wenyi Wu[c], Xiongwei Wu[a,*], Weiping Tang [b,*] and Yuping Wu[a,c,d*]

Received 00th January 2015,
Accepted 00th January 2015

DOI: 10.1039/x0xx00000x

www.rsc.org/

Abstract: $LiNi_{0.8}Co_{0.15}Al_{0.05}O_2$ is considered as an alternative for commercial $LiCoO_2$ positive electrode material for lithium ion batteries because of its excellent cycling performance. However, its capacity fading and potential safety hazard still need to be improved. In this study, fluorination has been introduced for the first time to modify the surface of $LiNi_{0.8}Co_{0.15}Al_{0.05}O_2$ by a one-step facile and dry method. The crystalline structure, morphology, surface information and electrochemical performance were characterized by X-ray diffraction, scanning electron microscopy and X-ray photoelectronic spectroscopy and electrochemical tests. The surface-fluorinated $LiNi_{0.8}Co_{0.15}Al_{0.05}O_2$ exhibits a reversible capacitance up to 220.5 mAh g^{-1} at 0.1C, good rate capability, and an excellent long-term cycling stability with 93.6% capacity retention after 80 cycles at 0.1C, which is much better than the pristine commercial $LiNi_{0.8}Co_{0.15}Al_{0.05}O_2$. The main reason is that metal-fluorine (M-F) bond partially replaces the metal-oxygen (M-O) bond at the surface, enhancing the entire bond energy as well as the structure stability. In addition, the interfacial conductivity between the electrolyte and the positive electrode has been increased, leading to a faster kinetic process. These results show that fluorinated $LiNi_{0.8}Co_{0.15}Al_{0.05}O_2$ is a promising positive electrode material for high performance lithium ion batteries.

Introduction:

In recent years, lithium ion batteries have played an important role in the field of advanced alternative power sources for portable electronics, electric vehicles (EVs) and plug-in hybrid electric vehicles (PHEVs) applications because of their high energy and power densities, satisfactory safety, long cycling life and environmental friendliness.[1-4] $LiCoO_2$ is the most extensively applied in commercial lithium ion batteries among various positive electrode materials, but its further application has been limited by its relative low capacity (~145 mAh/g, only 50% of its theoretical capacity) and high cost because of the expensive element Co.[5-7] So alternatives of high capacity and outstanding cycling performance should be searched.

$LiNiO_2$ has long been considered as a substitute for $LiCoO_2$ for lithium ion batteries. It has a similar layered structure like $LiCoO_2$ and higher reversible capacity (>180 mAh/g). [8,9] However, its application suffers from the fragile layered structure caused by Li/Ni cation mixing. Moreover, there is little prospect of producing $LiNiO_2$ on a large scale due to the generation of Li-deficient compounds (Li_dNiO_{2-d}, $0 < d < 1$), resulting from the easy decomposition of $LiNiO_2$. [10] Solutions to this problem have been widely studied and it is proved that the most effective strategy is substituting Ni^{3+} by a small certain amount of Co^{3+} and Al^{3+} to form $LiNi_aCo_bAl_{1-a-b}O_2$ (NCA, $1 > a > b > 0$) solid solution since the introduced Co and Al can improve the structure stability by controlling phase changes during the charging and discharging processes. [11-14] Although the electrochemical performance and the thermal stability have been improved, NCA still needs improvement to satisfy the requirements of high performance lithium ion batteries. [15] At the end of the charging process, unstable Ni^{4+} existing in the highly delithiated such as $Li_{1-d}Ni_{0.8}Co_{0.15}Al_{0.05}O_2$ will quickly transform to a more stable NiO-type rock salt phase by releasing oxygen through the decomposition of NCA, which results in capacity fading and potential safety hazard. [16]

[a] College of Science, Hunan Agriculture University, Changsha, Hunan 410128, China, Email: wxwcsu05@aliyun.com.
[b] Shanghai Institute of Space Power Sources (SISP), Shanghai Academy of Spaceflight Technology, Shanghai 200233, China. Email: *wptang1962@gmail.com*; Tel: +86-21-24187672
[c] New Energy and Materials Laboratory (NEML), Department of Chemistry & Shanghai Key Laboratory of Molecular Catalysis and Innovative Materials, Fudan University, Shanghai 200433, China. E-mail: *wuyp@fudan.edu.cn*; Tel/Fax: +86-21-5566 4223.
[d] College of Energy, Nanjing Tech University, Nanjing 211816, Jiangsu Province, China.

To solve these aforementioned problems, the most common and effective approach has been reported is to coat the NCA positive electrode material with a uniform layer like carbon materials,[17,18] metal oxides, [19-21] metal phosphates, [22,23] and other positive electrode materials.[24-27] These coating layers can be considered as protective layers to reduce the direct contact between the positive electrode materials and the non-aqueous electrolyte or the atmosphere, further improving the cycling performance. However, a common problem of these coatings is that the coating layer cannot tightly adhere the core material. Especially, long time cycling will lead coating layer to strip from the mother matrix. Moreover, most of the coated positive electrode materials are based on the wet process, which uses aqueous or nonaqueous solvents (mostly alcohol) and requires additional and complicated coating processes of mixing, drying, and heating. The high production cost and wet circumstance in this process are not suitable for NCA. Hence, a new surface modification method with a simple dry process for positive electrode materials has been recently reported: surface fluorination. [28-31]

Here, to our knowledge, we reported for the first time a modification on NCA positive electrode material by a one-step, facile and dry surface fluorination method. It is known that the electronegativity of F is the strongest among all the elements, leading to the strongest electrophilic ability. The metal-fluorine (M-F) bonds replace partial metal-oxygen (M-O) bonds at the surface, improving the bond energy as well as the structure stability. [32] The modified positive electrode material shows excellent electrochemical performance, and is of great promise for practical application.

Experimental

Fabrication of the surface-fluorinated NCA sample

The pristine NCA sample was commercially supplied from Toda Co. Ltd., Japan. To obtain a surface-fluorinated NCA sample, a certain amount of NH_4F was added to the pristine NCA with the atomic ratio of 1:100 (F: NCA). After well mixing for half an hour with the use of agate mortar, the prepared mixture was annealed for 2 h around 300°C to 700°C.

Materials characterization

Crystal structures of the samples were measured by a Rigaku D/MAX-IIA X-ray diffractometer (XRD) with Cu-K_α radiation. Scanning electron microscopy (SEM) was used to characterize the morphology of the pristine NCA sample and the surface-fluorinated NCA samples. The micrographs were obtained on a Philips XL30 scanning electron microscope. X-ray photoelectron spectroscopy (XPS, PHI5600, Perkine Elmer) measurements were carried out to get surface information of the surface-fluorinated NCA sample.

Electrochemical test

To prepare the positive electrode, the as-prepared samples, poly(vinylidene fluoride) (binder) and Super P carbon (conductive agent) were blended at a weight ratio of 8:1:1 with the help of N-pyrrolidinone (NMP), and then the resulting slurry was coated onto an Al foil. The weight of the active material loaded on one electrode is about 4 - 5 mg, which was precisely weighed prior to assembling into cells. After drying at 120 °C under vacuum for 12 h, the electrodes were assembled into CR2025 coin-type cells with metallic lithium as the counter and reference electrode in an Ar-filled glove box. A solution of 1 M $LiPF_6$ in ethylene carbonate and ethyl methyl carbonate (EC: EMC = 3:7 volume) was used as the eelctrolyte. Celgard 2400 polypropylene membrane was used as the separator. LAND battery test system was employed to test galvanostatic charging-discharging behavior and the cycling performance with the potential window ranging from 2.8 to 4.3 V (vs. Li^+/Li) at 0.1C rate (0.1C corresponds to 18 mA g^{-1}). Cyclic voltammetry (CV) and the electrochemical impedance spectroscopy (EIS) were tested by Princeton Applied Research Potentiostat/Galvanostat Model 273A and Plus Solarton SI1260 impedance/gain-phase analyzer at room temperature. The CV test was investigated at the scan rate of 0.1 mV s^{-1} and the EIS was conducted under the frequency from 10^5 Hz to 0.1 Hz with an amplitude of 5 mV.

Results and discussion

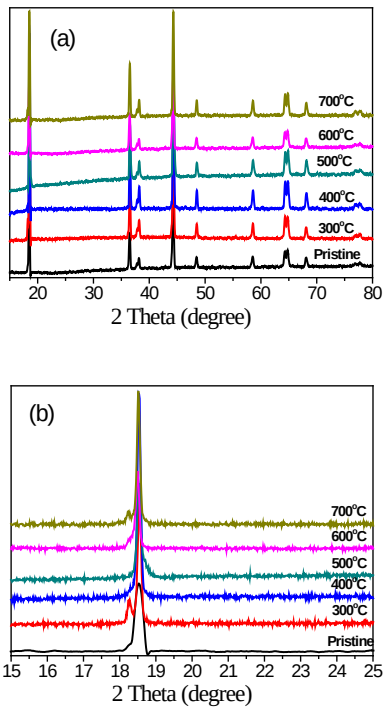

Fig. 1 (a) XRD patterns of the pristine NCA sample and the fluorinated NCA samples under different fluorinated temperatures from 300°C to 700°C, and (b) the magnified patterns of (a) between 15-25°.

Fig. 1a shows XRD patterns of the pristine NCA and the surface-fluorinated NCA heat-treated at 300-700°C. The samples fluorinated at 400-600°C exhibit the same diffraction peaks as those of the pristine NCA, these samples are single phase with isostructure of $LiNiO_2$, which adopts $R\bar{3}m$ space group. [33] However, when it is treated at 300°C or 700°C, an impure peak appeared at 18.2°, which can be clearly seen in Fig. 1b (the magnified pattern of Fig. 1a). The possible reason is that NH_4F has not been decomposed completely at 300°C while at 700 °C, the decomposed product from NH_4F may be introduced into the crystal lattice, causing the structural change.

Therefore, it is obvious that too high or too low heat-treated temperature is not favoured to modify the NCA.

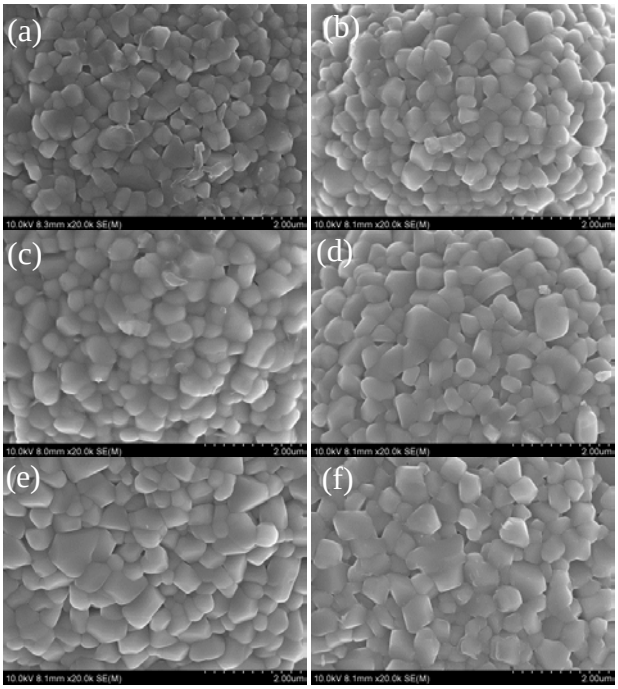

Fig. 2 SEM micrographs of the pristine NCA sample (a) and the fluorinated NCA samples under different fluorinated temperatures: (b) 300°C, (c) 400°C, (d) 500°C, (e) 600°C and (f) 700°C.

Fig. 2 shows SEM micrographs of the NCA samples untreated and heat-treated at different temperatures. No obvious morphology change was observed for the surface of the NCA particles. That means the fluorination cannot damage the general morphology of the NCA particles. However, with the increase of the heat-treatment temperature, the average particle size have a growing tendency, that may be caused by the aggregation of tiny particles during the heat-treatment process, suggesting the exorbitant heat-treatment temperature is not suitable for the surface fluorination.

The charge and discharge curves of the pristine and the surface fluorinated NCA under different fluorinated temperatures from 300 °C to 700 °C in the first cycle are shown in Fig. 3a. The shapes of the discharge curves are similar to each other. However, the initial reversible capacities are different. The sample fluorinated at 400 °C delivers the highest initial capacity of 205.8 mAh/g. In addition, the coulombic efficiency for the first cycle also changes with the fluorinated temperature. At the lower temperatures of 300°C and 400°C, the efficiency is increased from 82.7% for the pristine NCA sample to 86.8% and 84.6%, respectively. However, when the fluorinated temperature is up to 500 °C or 600°C, it is decreased, on the contrary, even down to 69% when the fluorinated temperature is 700°C. The phenomenon proves that the lower fluorinated temperature is helpful to improve the coulombic efficiency. Besides, after stabilization, the NCA sample fluorinated at 400°C still presents the highest capacity of 220 mAh/g (as shown in Fig. 3b). On the basis of the above XRD patterns and SEM micrographs, it can be concluded that the optimum fluorination temperature would be 400°C, and the following results are based on the surface-fluorinated NCA sample heat-treated at 400°C

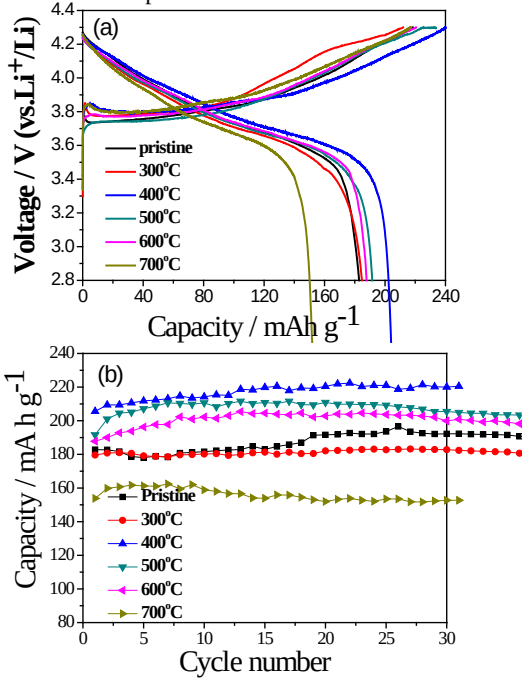

Fig. 3 (a) The initial charge and discharge curves and (b) cycling performance of the pristine and surface fluorinated NCA under different fluorinated temperatures from 300 °C to 700 °C.

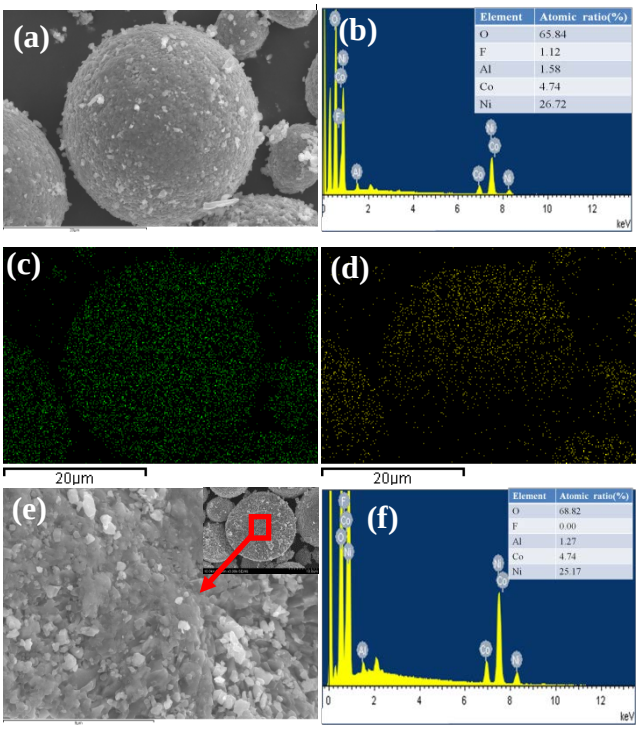

Fig. 4 (a) SEM micrographs of the surface-fluorinated NCA sample from heat-treatment at 400°C , (b) the EDS spectrum of the surface-fluorinated NCA sample, the EDS mapping of (c) Ni and (d) F, (e) the cross-section SEM micrographs of the surface-fluorinated NCA sample and (f) the EDS spectrum of the cross-section.

The energy dispersive spectrometer (EDS) was employed to know the surface information of the surface-fluorinated NCA sample, and results are shown in Fig.4. As seen from Fig. 4a, the surface-fluorinated NCA sample shows a spherical and smooth morphology, which is the same as that of the pristine one. EDS spectrum (Fig. 4b) displays the presence of F elements, and the atomic ratio of F in the sample is 1.12%, which is in agreement with the addition amount of F. It is difficult to distinguish the thickness of the fluorine layer from the SEM micrograph. From Fig. 4c and 4d, it can be seen that the green and yellow dots assigned to Ni and F elements, respectively, are uniformly distributed on the surface of the NCA sample. Besides, to further verify the added F is at the surface of the positive electrode, the EDS measurement was also carried out for the cross-section of the surface-fluorinated NCA sample (Fig. 4e), and the EDS spectrum was shown in Fig. 4f. It is found that the atomic ratio of F for the cross-section is nearly 0.00%, indicating there is almost no F element in the bulk, only at the surface of the NCA sample, which is helpful to protect NCA particles from the side reactions between NCA and electrolytes or air.

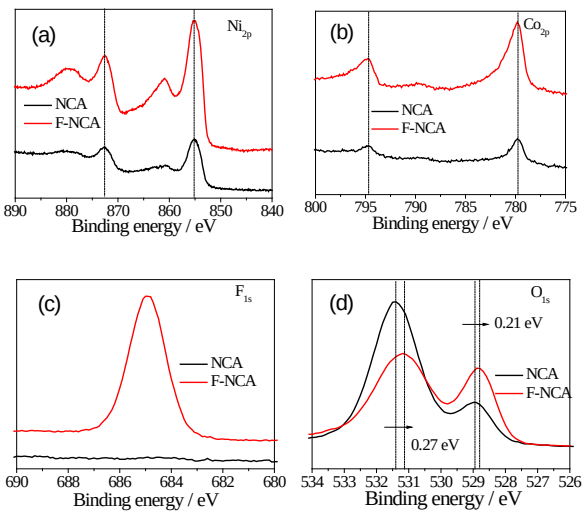

Fig. 5 XPS analysis of the pristine NCA and the surface-fluorinated NCA sample from the heat-treatment at 400°C (F-NCA): (a) Ni_{2p}; (b) Co_{2p}; (c) F_{1s}; and (d) O_{1s}.

XPS analysis of the pristine NCA and the surface-fluorinated NCA was carried out and the related spectra are shown in Fig. 5. In the spectra of Ni_{2p} and Co_{2p} (Fig. 5a and 5b), the peaks of the surface-fluorinated NCA sample are identical with the pristine NCA, indicating there is little change on the bulk M-O bondage.[34] Fig. 5c (the spectrum of F_{1s}) obviously shows that the peak at 685 eV appears after the fluorination, indicating that fluorine is successfully introduced at the surface of NCA. It is reported that the 685 eV is the binding energy for F^- in the solid samples such as alkali metal fluorides. So, the peak at 685 eV can be considered as the result of the interaction between F^- and ionic metal elements in the NCA sample. For O_{1s} spectrum, there are two peaks for both the pristine NCA and the surface-fluorinated NCA. As reported, the peak located at 528 - 530 eV can be assigned to the lattice oxygen in the metal framework such as M^{3+}-O at the surface, while the peak located at the higher binding energy of 531~533 eV can be attributed to the chemical adsorbed species (such as LiOH or Li_2CO_3).[35-37] In addition, it is interesting to notice that after the fluorination, both peaks at low and high binding energies shift to lower binding energy for 0.21 and 0.27 eV, respectively. That is to say, the chemical adsorbed oxygen has been decreased, confirming indirectly O has been partly replaced by F. Moreover, the ratio of the intensity of the peaks at high and low binding energies decreases distinctly after the surface fluorination. In another word, the lattice oxygen becomes more while the absorbed oxygen becomes less relatively in the surface-fluorinated NCA sample. In addition, the pristine NCA and the surface-fluorinated NCA with the same amount (1.0 g) were put in the atmosphere with different humidity for 12 hours, their absorbed water content were tested by Karl-Fischer method, and the results are shown in Fig. 6. It is obvious that the water content is greatly diminished after the surface fluorination. What's more, with the increase of the air humidity, the growth tendency of the absorbed water is restrained. These demonstrate that fluorine is successfully located at the surface of NCA particle and this modification will not only protect the M-O bond from the attack of HF, which is produced by the hydrolysis of the $LiPF_6$ with a small amount of residual water, but also inhibit the side reaction between the surface of NCA particles and H_2O or CO_2 in the air.

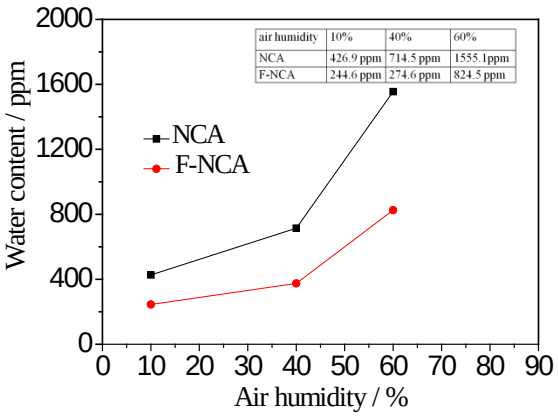

Fig. 6 The change of absorbed water content for the pristine NCA and the surface-fluorinated NCA after storage in an atmosphere of different humidity.

Fig. 7a shows the initial charge-discharge curves of the pristine and the surface fluorinated NCA at a current density of 18 mA g^{-1} (0.1C) in the voltage window of 2.8-4.3 V. The shape of the curves for two samples is almost similar, indicating that fluorine is not introduced into the bulk of the NCA, which is in accordance with XRD results. The initial discharge capacity of the pristine NCA is 182.8 mAh g^{-1}, while that of the surface-fluorinated NCA is 205.8 mAh g^{-1}. Fig.7b shows the 20th charge/discharge curves of the pristine and surface-fluorinated NCA. It can be seen that the capacities of both samples are increased. This is also due to an activation and infiltration process during the initial cycling. In addition, the discharge voltage for the surface-fluorinated NCA is slightly higher than that of the pristine NCA, which is due to the increased interfacial conductivity, leading to a lower polarization. Fig. 7c displays the cycling performances of the two samples. Apparently, the surface-fluorinated NCA presents much higher capacity than the pristine one during the cycling. After 80 cycles the pristine NCA sample delivers 163.7 mAh g^{-1}, which is as much as

83.3% of its maximum capacitance after stablization. In contrast, the surface fluorinated NCA delivers a capacity of 205.3 mAh g^{-1} after 80 cycles and its capacity retention is 93.1% of the maximum (220.5 mAh g^{-1}). It is reasonable to conclude that the surface-fluorination can enhance markedly the structure stability and cycling performance, resulting from the protected M-O by M-F. To more easily illustrate the enhanced electrochemical property, the rate capabilities at various current densities are shown in Fig. 7d. The surface-fluorinated NCA almost delivers higher discharge capacities than the pristine one at all the current densities, especially at high rates. In particular, the surface-fluorinated NCA exhibits the capacity of 191.1 mAh g^{-1} at 1 C, in comparison with 169.1 mAh g^{-1} for the pristine material. The dramatic improvement of the discharge capacity is mainly attributed to the increase of electric conductivity at the surface between the electrolyte and the positive electrode resulting from the introduction of fluorine, which serves as a fast electron transference and a fast lithium ion diffusion channels on the surface of the positive electrode, in favor of the faster solvation/desolvation of the lithium ion proceeds.[38-40] It is known that electrochemical redox reactions usually take place at the interface between the electrolyte solution and the electrode. The fluoride anion has a greater interaction with the Li^+ ion than the oxide anion, it is expected that the M-F bond at the surface of the positive electrode-active material promotes the Li^+ ion transference at the interface between the active electrode material and the electrolyte solution where the Li^+ ion is solvated. Therefore, the transference of Li^+ ion between the solid and the liquid phases can easily take place.

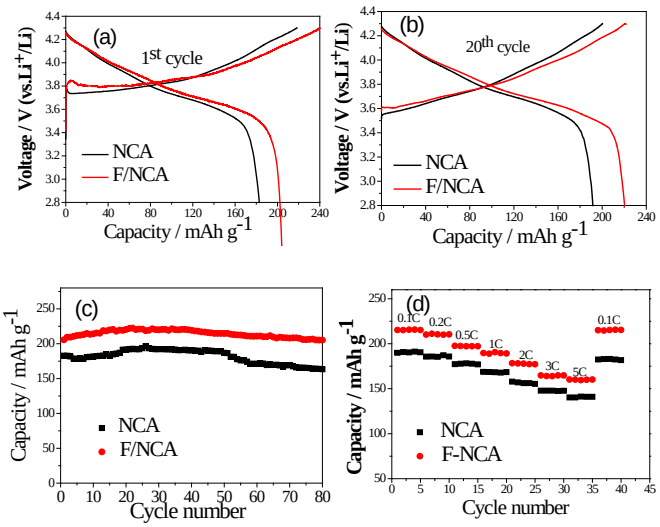

Fig. 7 (a) The initial charge/discharge curves of the pristine NCA and the surface-fluorinated NCA sample from the heat-treatment at 400 °C at 0.1 C; (b) the charge/discharge curves in the 20th cycle of the pristine NCA and the surface-fluorinated NCA sample at 0.1 C; (c) the cycling performance of the pristine NCA and the surface-fluorinated NCA sample at 0.1 C; and (d) the discharge capacities of the pristine and the surface-fluorinated NCA sample at various current densities (0.1 C-5 C).

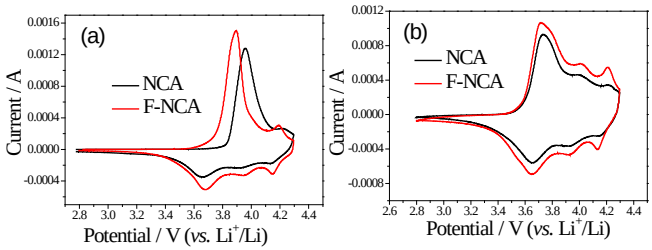

Fig. 8 Cyclic voltammograms of the pristine NCA and the surface-fluorinated NCA from the heat-treatment at 400°C: (a) before cycling and (b) after 30 cycles.

Fig. 8 shows the cyclic voltammograms (CVs) for the pristine and the surface-fluorinated NCA at room temperature in the voltage range of 2.8-4.3 V at the scan rate of 0.05 mV s^{-1}. In general, the peaks in the CV curves correspond to redox reactions upon lithium insertion and extraction. It can be seen that the electrochemical redox couples of transition metal ions are not changed after the surface fluorination. Before cycling, the obtained initial CV curve of the surface-fluorinated NCA sample is almost identical to that of the pristine NCA sample. However, the oxidation peak in the first scan occurs at a lower voltage (3.85 V) than that of the pristine NCA (3.95 V) while the reduction peak occurs at a higher voltage (3.67 V) than that of pristine NCA (3.64 V). That means the potential difference of the oxidation and reduction peaks is decreased after the surface fluorination, indicating the reduced resistance and the improved reversibility of the NCA positive electrode materials. For further investigation, both the assembled cells with the pristine and surface-fluorinated NCA as positive materials after 30 cycles were further characterized by CV test. As shown in Fig. 8b, after 30 cycles the surface-fluorinated NCA shows the more obvious and sharp redox peaks than those of the pristine NCA, further proving the promoted reversibility and cycling performance. The major anodic/cathodic peaks at 3.65/3.71 V are ascribed to the oxidation/reduction process of Ni^{3+}/Ni^{4+}. Also the anodic/cathodic peaks at 3.94/3.99 V and 4.13/4.20 V are assigned to the phase transition. [18] In addition, whether the first cycle or after 30 cycles, the surface modified NCA electrodes show much larger area of the CV curves than the pristine one, telling that the surface-fluorinated NCA can deliver higher reversible capacity, which is consistent with the above results.

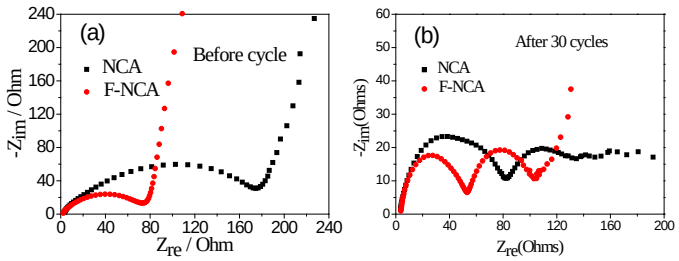

Fig. 9 EIS spectra of the pristine NCA and the surface-fluorinated NCA after the heat-treatment at 400 °C: (a) before cycling, (b) after 30 cycles.

Fig. 9a shows the EIS spectra of the pristine and the surface-fluorinated NCA before cycling. Both spectra have the high-frequency semicircles and low-frequency tails. The semicircle is attributed to the charge-transfer resistance (R_{ct}). The EIS measurement are also carried out after 30 cycles, which is shown in Figure 9b. Another semicircle appeared in the intermediate-frequency, assigning to the surface-film resistance (R_{sf}), which is mainly formed during the initial charge/discharge processes. It is seen that after the surface fluorination, both R_{sf} and R_{ct} are smaller than those of the pristine NCA. This is perhaps attributed to two reasons: (1) the dissolution of active ion by acid species taking place at the electrolyte/electrode interface is decreased, and (2) the surface film formed on the electrode is more compatible with the electrolyte. [38-40] The EIS measurement demonstrates a faster kinetic process of the surface treated NCA samples, leading to the enhanced performance, which is consistent with the results in Fig.7d.

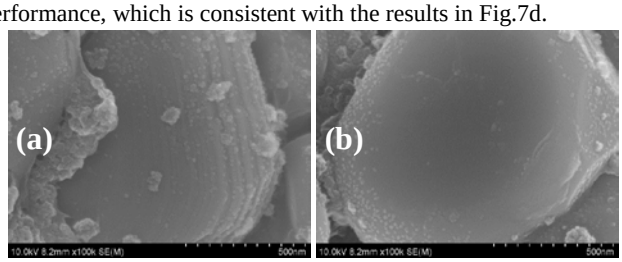

Fig. 10 SEM micrographs of (a) the pristine NCA and (b) the surface-fluorinated NCA from the heat-treatment at 400°C after 80 cycles.

Fig. 10 shows the SEM micrographs for the pristine and the surface-fluorinated NCA after 80 cycles. The surface of the pristine material becomes coarse. It might be caused by the dissolution of the transition metal ions at the particle surface resulting from HF attack in the electrolyte and the deposition of the decomposition products of the electrolyte during the cycling. In contrast, the surface-fluorinated NCA samples is still very smooth, which means the introduced fluorine can avoid the side-reactions between the positive electrode materials and electrolyte, further decreasing the structure degradation, and this is the main reason why the surface-fluorinated NCA sample provides improved cycling performance.

Conclusions

In summary, the surface-fluorinated NCA positive electrode material has been successfully prepared by a one-step facile and dry method. When the fluorinated temperature is 400°C, the surface modification NCA sample shows the best electrochemical performance. At 0.1C, the initial discharge capacity can reach 205.8 mAh g^{-1} in the voltage range from 2.8 to 4.3 V (vs. Li^+/Li), and up to 220.5 mAh g^{-1} after stabilization. In addition, the surface-fluorinated NCA still delivers a capacity of 205.3 mAh g^{-1} after 80 cycles and its capacity retention is 93.1%, much better than that of the pristine NCA (83.3%). The excellent electrochemical performance is attributed to the surface modification, where the metal-fluorine (M-F) bond replaces the metal-oxygen (M-O) bond partially at the surface, improving the entire bond energy as well as the structure stability. In addition, the introduction of F can protect the M-O bond from the side reaction with the electrolyte and atmosphere, reducing the release of O from the space lattice and enhancing the safety performance. In addition, the fluoride anion has a greater interaction with the Li^+ ion than the oxide anion, resulting in faster transference of Li^+ ion between the active material and the electrolyte and the lower charge transfer resistance. It is clear that the surface-fluorinated NCA sample with improved electrochemical performance is a promising positive electrode material for lithium ion batteries.

Acknowledgement: Financial support from rom China National Distinguished Youth Scientists (NSFC No. 51425301) and STCSM (No. 14520721800) is greatly appreciated.

References:

1 Y. M. Chiang, *Science*, 2010, **330**, 1485-1486.
2 E. J. Yoo, J. Kim, E. Hosono, H. Zhou, T. Kudo, I. Honma, *Nano Lett.*, 2008, **8**, 2277-2282.
3 J. M. Tarascon, M. Armand, *Nature*, 2001, **414**, 359-367.
4 V. Etacheri, R. Marom, R. Elazari, G. Salitra, D. Aurbach, *Energy Environ. Sci.*, 2011, **4**, 3243-3262.
5 T. Wei, R. Zeng, Y. M. Sun, Y. H. Huang, K. V. Huang, *Chem. Commu.*, 2014, **50**, 1962-1964.
6 H. H. Nie, L. Xu, D. W. Song, J. S. Song, X. X. Shi, X. Q. Wang, L. Q. Zhang, Z. H. Yuan, *Green Chem.*, 2015, **17**, 1276-1280.
7 R. Robert, C. Villevieille, P. Novák, *J. Mater. Chem. A*, 2014, **2**, 8589-8598.
8 Arai, M. Tsuda, K. Saito, *Electrochimca. Acta*，2002, **47**, 2697-2705.
9 Z. C. Liu, H. H. Zhen, Y. Kim, C. D. Liang, *J. Power Sources*, 2011,**196**, 10201-10206.
10 T. Nonaka, C. Okuda, Y. Seno, Y. Kondo, K. Koumoto, Y. Ukyo, *J. Electrochem. Soc.*, 2007, **154**, A353-358.
11 A. G. Ritchie, C. O. Gowa, J. C. Lee, *J. Power Sources*, 1999, **80**, 98-102.
12 J. S. Weaving, F. Coowar, D. A. Teagel, *J. Power Sources*, 2001, **97**, 733-735.
13 S. H. Ju, H. C. Jang, Y. C. Kang, *Electrochim. Acta*, 2007, **52**, 7286-7292.
14 H. Kondo, Y. Takeuchi, T. Sasaki, *J. Power Sources*, 2007, **174**, 1131-1136.
15 N. Kimiaie, K. Wedlich, M. Hehemann, R. Lambertz, M. Muller, C. Korte, D. Stolten, *Energy Environ. Sci.*, 2014, **7**, 3013-3025
16 D. P. Abraham, R. D. Twesten, M. Balasubramanian, I. Petrov, J. McBreen, K. Amine, *Electrochem. Commun.* 2002, **4**, 620-625.
17 Y. M. Chung, S. H. Ryu, J. H. Ju,Y. R. Bak, M. J. Hwang, K. W. Kim, K. K. Cho, K. S. Ryu, *Bull. Korean Chem. Soc.*, 2010, **31**, 82304-82308
18 S. Yoon, K. N. Jung, S. H. Yeon, C. S. Jin, K. H. Shin, *J. Electroanal. Chem.*, 2012, **683**, 88.
19 Y. Cho, J. Cho, *J. Electrochem. Soc.*, 2010, **157**, A625-A629.
20 Y. Cho, Y. S. Lee, S. A. Park, *Electrochimica. Acta*, 2010, **56**, 333-339.
21 S. B. Xia, Y. J. Zhang, P. Dong, Y. N. Zhang, *Eur. Phys. J. Appl. Phys.*, 2014, **66**, 30403
22 D. J. Lee, B. Scrosati, Y. K. Sun, *J. Power Sources*, 2011, **196**, 7742-7746.

23 B. Huang, X. H. Li, Z. X. Wang, H. J. Guo, *Mater. Lett.*, 2014, 131, 210-213.
24 W. Liu, G. Hu, K. Du, *Surf. Coat. Tech.*, 2013, **216**, 267-272.
25 K. S. Lee, S. T. Myung, Y. K. Sun, *J. Power Sources*, 2010, **195**, 6043-6048.
26 Y. Seino, T. Ota, K. Takada, *J. Power Sources*, 2011, **196**, 6488-6492.
27 J. H. Ju, R. K. Sun, *J. Alloy. Compd.*, 2011, **509**, 7985-7992.
28 T. Nakajima, A. Ueno, T. Achiha, Y. Ohzawa, M. Endo, *J. Fluorine Chem.*, 2009,**130**, 810–815
29 S. Yonezawa, M. Yamasaki, M. Takashima, *J. Fluorine Chem.*, 2004, **125**, 1657-1661.
30 P. F. Fulvio, G. M. Veith, J. L. Adcock, S. S. Brown, R. T. Mayes, X. Q. Wang, S. M. Mahurin, B. K. Guo, X. G. Sun, A. A. Puretzky, C. M. Rouleau, D. B. Geohegan, S. Dai, *J. Mater. Chem. A*, 2013, **1**, 9414-9417
31 Z. C. Zhang, L. B. Hu, H. M. Wu, W. Weng, M. T. Koh, P. C. Redfern, L. A. Curtiss, K. Amine, *Energy Environ. Sci.*, 2013, **6**, 1806-1810
32 H. Z. Yang, P. X. Liu, Q. L. Chen, X. W. Liu, Y. W. Lu, S. F. Xie, L. Ni, X. Y. Wu, M. Y. Peng, Y. B. Chen, Y. F. Tang, Y. F. Chen, *RSC Adv.*, 2014, **4**, 35522-35527.
33 W. S. Yoon, K.Y. Chung, J. McBreen, X.Q. Yang, Electrochem. Commun., 2006, **8**, 1257.
34 T. Nonaka, C. Okuda, Y. Seno, K. Koumoto, Y. Ukyo, *Ceram. Int.*, 2008, **34**, 859-862.
35 A. M. Andersson, D. P. Abraham, R. Haasch, S. MacLaren, J. Liu, K. Amine, *J. Electrochem. Soc.*, 2002, **149**, A1358.
36 N.V. Kosova, E.T. Devyatkina, V.V. Kaichev, *J. Power Sources*, 2007,**174**, 965.
37 S. C. Yin, Y. H. Rho, I. Swainson, L. F. Nazar, *Chem. Mater.*, 2006, **18**, 1901.
38 W. Choi, A. Manthiram, *J. Electrochem. Soc.*, 2008, **154**, A792-A797.
39 Y. Wu, A. Manthiram, *Solid State Ionics*, 2009, **180**, 50-56.
40 H. S. Shin, D. W. Shin, Y. K. Sun, *Electrochimica Acta*, 2006, **52**, 1477-1482.

Table of content:

Surface fluorinated $LiNi_{0.8}Co_{0.15}Al_{0.05}O_2$ as positive electrode material for lithium ion batteries

Lei Zhu, Yang Liu, Wenyi Wu, Xiongwei Wu, Weiping Tang and Yuping Wu

A surface-fluorinated NCA is prepared for the first time by a one-step facile and dry method, and it exhibits higher capacity, better rate capability and excellent cycling stability.